Control of the glass-liquid transition temperature in $YBa_2Cu_3O_{7-x}$ films

Tomoya Horide
Department of Materials Science and Engineering, Kyoto University, Yoshida-honmachi, Sakyo-ku, Kyoto 606-8501, Japan

Kaname Matsumoto* and Paolo Mele
Department Materials Science, Kyushu Institute of Technology, Kitakyushu 804-8550, Japan

Yutaka Yoshida
Department of Energy Engineering and Science, Nagoya University, Nagoya 464-8603, Japan

Ataru Ichinose
Electric Power Engineering Research Laboratory, Central Research Institute of Electric Power Industry, Nagasaka, Yokosuka, Kanagawa 240-0196, Japan

Ryusuke Kita
Graduate School of Science and Technology, Shizuoka University, Hamamatsu, Shizuoka 432-8651, Japan

Shigeru Horii
Department of Applied Chemistry, University of Tokyo, Tokyo 113-8656, Japan

Masashi Mukaida
Department of Material Science and Engineering, Kyushu University, Fukuoka 819-0395, Japan
(Received 30 August 2008; revised manuscript received 8 December 2008; published 10 March 2009)

Magnetic field dependences of the glass-liquid transition temperature (T_g) were studied in $YBa_2Cu_3O_{7-x}$ films containing various types of nanoinclusions. The vortex configuration (entangled or straight) and pinning strength for each vortex are crucial to the behaviors of T_g. *c*-axis correlated pinning centers optimize these factors and achieve the upper limit of T_g, which is determined by loss of line tension of vortices, if they are elongated through a thickness of a sample. By optimizing pinning centers, critical temperature, and a matching field, a T_g value of 77 K can be obtained in $YBa_2Cu_3O_{7-x}$ in a magnetic field as high as 27 T.

DOI: 10.1103/PhysRevB.79.092504 PACS number(s): 74.25.Qt, 74.72.Bk, 74.78.Bz

Quantized vortices in high-temperature superconductors exhibit rich vortex phases, and the glass-liquid transition is important matter in vortex physics.[1] Since thermal fluctuation, line tension of vortices, interaction between vortices, and pinning centers affect the glass-liquid transition, behaviors of the glass-liquid transition are complicated. Two kinds of the glass-liquid transitions [the Bose glass (BG) transition[2–4] and the vortex glass (VG) transition[5,6]] are actively studied in order to clarify the behaviors of the glass-liquid transition.

One of the most important issues on the glass-liquid transition is the upper limit of the glass-liquid transition temperature (T_g).[7] By evaluating vortex behaviors in the vortex liquid phase using a flux transformer experiment, it was concluded that the upper limit of T_g was determined by the loss of line tension of vortices.[7] However, since the upper limit of T_g was not sufficiently discussed based on the glass-liquid transition, the influence of the loss of line tension of vortices on T_g is still unclear. In addition, a question also arises as to what kind of pinning centers achieve the upper limit of T_g. In order to clarify this matter, the upper limit of T_g should be discussed based on experimental results on the glass-liquid transition. The upper limit of T_g is important also from technological points of view. Various types of artificial pinning centers were incorporated into $YBa_2Cu_3O_{7-x}$ (YBCO) coated conductors (CCs) to enhance their vortex pinning properties.[8–10] It is true that the vortex pinning in CCs was improved,[8–10] but superconductor applications would always expect higher and higher performance CCs. Therefore, the upper limit of the vortex pinning (the upper limit of T_g) should be clarified in order to set the final goal on the control of vortex pinning in CCs and to enhance the performance of CCs as much as possible.

In this Brief Report, magnetic field dependences of T_g in YBCO films containing various types of pinning centers were measured in order to discuss influence of the pinning centers on T_g-*B* curves. Based on the experimental results, we discuss the upper limit of T_g and clarify conditions for the upper limit of T_g.

YBCO+$BaZrO_3$ (BZO) (0.5, 1.5, and 4 wt %) single layer films (SLs), an YBCO+$BaSnO_3$ (BSO) (4 wt %) SL, YBCO+BZO (4 wt %)/YBCO multilayer films (MLs), an YBCO+Y_2O_3 (5 areal %) film, and a "pure" YBCO film (i.e., a film without artificially introduced nanoinclusions) were prepared on single-crystal $SrTiO_3$ substrates using pulsed laser deposition (PLD). Thicknesses of the YBCO+BZO (4) SL, the YBCO+BZO (4)/YBCO MLs, the YBCO+Y_2O_3 film, and the pure YBCO film are 350–400 nm. Thicknesses of the YBCO+BSO (4) SL and the YBCO+BZO (0.5, 1.5) SLs are 230 and 320 nm, respectively. T_c values of the films are 86.4–89.9 K. T_g was defined as the temperature at which a concavity in a double-

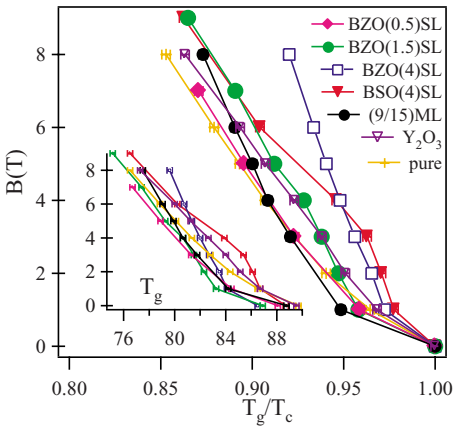

FIG. 1. (Color online) T_g/T_c-B curves in the YBCO+BZO (0.5, 1.5, 4) SLs, the YBCO+BSO (4) SL, the (9.2 nm/15.5 nm) ML, the YBCO+Y_2O_3 film and the pure YBCO film. Error bars are in most cases smaller than their data points. Inset shows the T_g-B curves in the films.

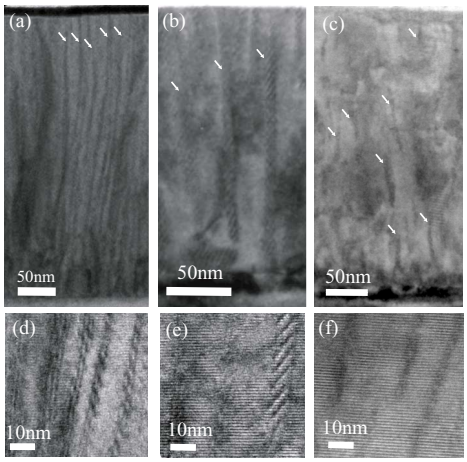

FIG. 2. TEM images of (a) the YBCO+BZO (4) SL, (b) the YBCO+BSO (4) SL, and (c) the YBCO+BZO (1.5) SL. (d), (e), and (f) are the enlarged views of (a), (b), and (c). Arrows show the BMO nanorods.

logarithmic plot of current density-electric field curves changed.[11]

T_g/T_c-B curves in the YBCO+BZO (4, 1.5, 0.5) SLs, the YBCO+BSO (4) SL, the YBCO+BZO (4)/YBCO (9.2 nm/15.5 nm) ML, the YBCO+Y_2O_3 film, and the pure YBCO film are presented in Fig. 1. As we will report later in this study, BMO (M=Zr,Sn) forms nanorods and Y_2O_3 forms isotropic nanoparticles in YBCO films. The BMO nanorods improved T_g/T_c most effectively in the YBCO+BZO(4) SL (in 0–9 T) and the YBCO+BSO(4) SL (in 0–3 T), but not in the YBCO+BZO (0.5, 1.5) SLs and the (9.2/15.5 nm) ML. Although the average concentrations of dopants in the YBCO+BZO (1.5) SL and in the (9.2/15.5 nm) ML are the same (1.5 wt %), their T_g/T_c values are clearly different as shown in Fig. 1. This suggests that the difference in T_g/T_c values in Fig. 1 results from morphology of the pinning centers, not directly from the average concentrations of dopants. Figure 2 reports transmission electron microscopy (TEM) images of the YBCO+BZO (4) SL, YBCO+BSO (4) SL, and YBCO+BZO (1.5) SL, respectively, showing the morphology of BMO nanorods in the films. The average diameters of the BMO nanorods in the YBCO+BZO (4) SL, the YBCO+BSO (4) SL, and the YBCO+BZO (1.5) SL are 3.3, 6.8, and 3.6 nm, respectively. Almost the same diameters of the BZO nanorods in the YBCO+BZO (4) SL and the YBCO+BZO (1.5) SL suggest that their difference in T_g/T_c values in Fig. 1 is not due to the diameters of the nanorods. As shown in Fig. 2, the elongation of the BZO nanorods was interrupted in the YBCO+BZO (1.5) SL because the amount of supply of BZO was small during the film deposition. On the other hand, the BMO nanorods are elongated nearly through the entire thicknesses of the films in the YBCO+BMO (4) SLs. Thus, the difference in the T_g/T_c values between the YBCO+BMO (4) SLs and YBCO+BZO (1.5, 0.5) SLs is due to the variation in the lengths of the BMO nanorods. Assuming that composition of BMO in the films is the same as that in the PLD targets, the BMO composition in the YBCO+BMO (4) SLs is 4 wt %. Thus, matching fields ($B_\Phi = n\phi_0$, where ϕ_0 is the flux quantum and n is a density of linear defects) can be obtained from the composition of BMO and the diameters of the BMO nanorods. The B_Φ values in the YBCO+BZO (4) SL and in the YBCO+BSO (4) SL are estimated to be 11.2 and 2.3 T, respectively. The results in Fig. 1 are consistent with the expected matching field effect[12] (a shoulder nearly at a B_Φ in T_g-B and T_{irr}-B curves, where T_{irr} is the irreversibility temperature). Thus, the BMO nanorods which are elongated through an entire thickness of a film are thought to be very effective pinning centers in magnetic fields lower than a B_Φ.

To discuss the mechanism that rules the high T_g/T_c in the YBCO+BMO (4) SLs in detail, T_g-B curves were systematically studied in well-organized model systems whose defect configuration, shape, and spatial distribution of pinning centers were controlled [Fig. 3(a)]. The detail of the model systems is explained in our previous paper.[11] The YBCO+Y_2O_3 film contains randomly distributed Y_2O_3 nanoparticles [an inset of Fig. 3(b)].[11] The BZO nanoinclusions are self-aligned along the c axis in the MLs [an inset of Fig. 3(c)].[11] In the MLs, lengths of the nanoinclusions, and spacing between them along the c axis can be varied.[11] Lateral spacing between the BZO nanoinclusions should be the same in the YBCO+BZO (4) SL and the MLs since all the same PLD conditions were used for the YBCO+BZO (4) layer deposition in the SL and the MLs. This is confirmed by the TEM images in Ref. 11 and in the present study [Figs. 2(a) and 2(d) and an inset of Fig. 3(c)]. Figures 3(b) and 3(c) show $\log_{10} B$ vs $\log_{10}(1-T_g/T_c)$ curves for the systems shown in Fig. 3(a). T_g-B curves are simply described by $B = B_0(1-T_g/T_c)^\alpha$, where B_0 is a proportionality constant and α is an exponent. α values in the pure YBCO, the YBCO+Y_2O_3, and the (9.2/15.5 nm) ML are 1.5, 1.4, and 2.3, respectively. The glass-liquid transition in pure YBCO films in high magnetic fields is dominated by the random point disorders (the VG).[11,13] The α value in the pure YBCO film reported in the present study is almost the same as that in the YBCO+Y_2O_3 film and is consistent with that for the VG in proton-irradiated bulk YBCO.[6]

Vortices are fixed by pinning centers below T_g. Therefore,

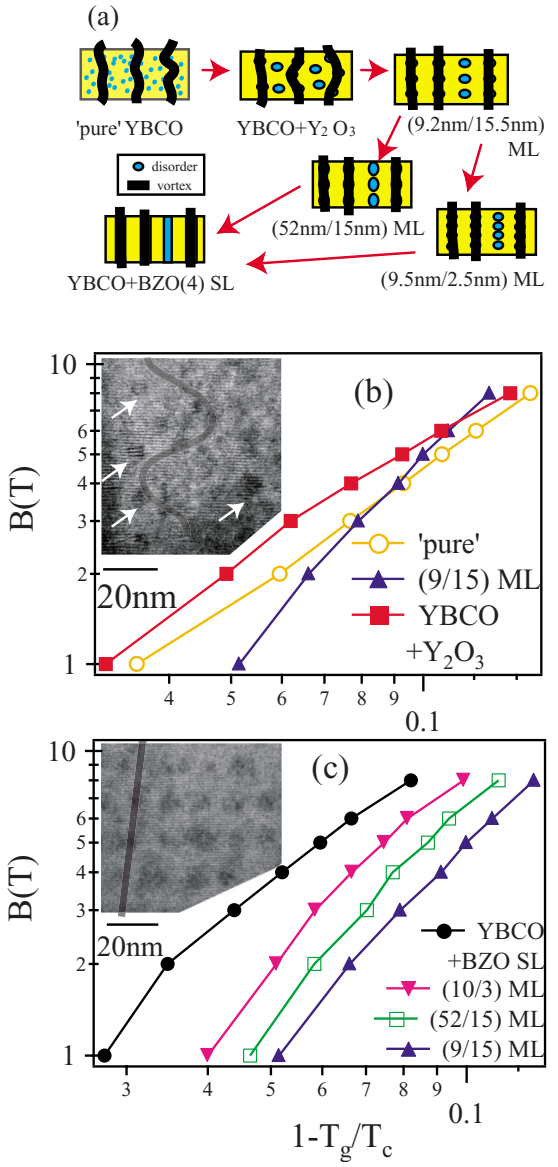

FIG. 3. (Color online) (a) Schematic images of model systems which are discussed in the present study. (b) Log_{10} B vs $\log_{10}$ $(1\text{-}T_g/T_c)$ curves in the pure YBCO, the YBCO+Y_2O_3, and the YBCO+BZO(4)/YBCO (9.2 nm/15.5 nm) ML. (c) Log_{10} B vs $\log_{10}$ $(1\text{-}T_g/T_c)$ curves in the (9.2 nm/15.5 nm) ML, the (9.5 nm/2.5 nm) ML, the (52 nm/15 nm) ML, and the YBCO+BZO (4) SL. Error bars are in most cases smaller than their data points. Insets in (b) and (c) show TEM images of the YBCO+Y_2O_3 film and the (8.4 nm/8 nm) ML. Arrows in the inset of (b) show Y_2O_3 nanoparticles. An entangled vortex configuration for the randomly distributed Y_2O_3 nanoparticles in the YBCO+Y_2O_3 and a straight vortex configuration for the ordered BZO nanoparticles in the ML are schematically illustrated on the TEM images in the insets of (b) and (c).

interaction between pinning centers and a vortex is crucial to T_g-B relations. An entangled vortex configuration is induced by the random point disorders in the pure YBCO film. Similarly, the entangled vortex configuration is induced by the randomly distributed Y_2O_3 nanoparticles as shown in the inset of Fig. 3(b). On the other hand, due to the self-aligned

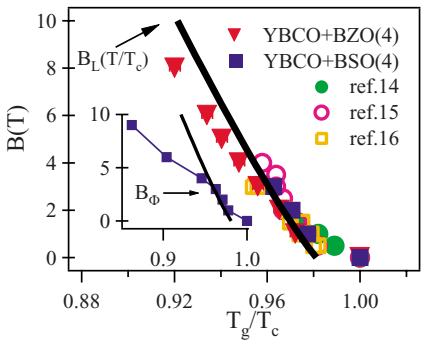

FIG. 4. (Color online) (a) T_g/T_c-B curves for $B<B_\Phi$ in the YBCO+BMO (4) SLs (the present study) and in heavy-ion irradiated YBCO films and bulk (previous reports, Refs. 14–16). A solid line shows a $B_L(T/T_c)$ curve given by Eq. (1). Inset shows the T_g/T_c-B curve in the YBCO+BSO (4) SL (B_Φ=2.3 T) and the $B_L(T/T_c)$ curve up to 9 T. Error bars are in most cases smaller than their data points.

BZO nanoparticles and the c-axis correlated BZO nanorods, vortices exhibit a straight configuration in the MLs as shown in the inset of Fig. 3(c). The vortex configuration (entangled or straight) was not changed between the pure YBCO and the YBCO+Y_2O_3, and their α values were almost the same. The elongated nanoparticles (short nanorods) and the closely packed self-aligned nanoparticles did not change the vortex configuration from that of the YBCO+BZO (4) SL and gave similar T_g/T_c-B behaviors to those in the YBCO+BZO (4) SL. However, the α value was markedly varied between the YBCO+Y_2O_3 film (α=1.4) and the (9.2/15.5 nm) ML (α =2.3), where the vortex configuration was considered to change from the entangled one to the straight one. This infers that the change in α may be due to the change of the vortex configuration. On the other hand, when pinning centers varied from the weak point disorders (the pure YBCO) to the strong Y_2O_3 nanoparticles (the YBCO+Y_2O_3 film), the T_g/T_c was enhanced. As the spacing between the BZO nanoinclusions decreased or their lengths increased along the c axis in the MLs, the T_g/T_c increased with the increase in the BZO fraction at each pinning site. Such enhancement in T_g/T_c is due to the increase in average pinning strength for each vortex. Thus, the vortex configuration (entangled or straight) and the pinning strength for each vortex are crucial to the T_g/T_c behaviors.

The sufficiently elongated BMO nanorods achieve the highest T_g/T_c in the present study as shown in Figs. 1 and 3. The possibility of further enhancement of the T_g in the YBCO+BMO SLs is considered as follows. Discussion of the upper limit should be based on T_g which is a thermodynamic quantity and not based on T_{irr}. It is expected that the upper limit of T_g can be achieved only in magnetic fields lower than a matching field. Figure 4 shows magnetic field dependences of T_g/T_c for $B<B_\Phi$ in the YBCO+BMO(4) SLs, in comparison to those in heavy-ion irradiated YBCO films and bulk which were reported by several authors.[14–16] The T_g/T_c-B curves in the present study are in good agreement with the previous ones as shown in Fig. 4. Samoilov *et al.*[14] concluded that their T_g/T_c-B data referred in Fig. 4 corresponded to the upper limit of T_g/T_c. Moreover, a char-

acteristic field, $B_L(T)$, above which the line tension of vortices becomes negligible, provides the theoretical upper limit of T_g.[7] $B_L(T/T_c)$ is given by

$$B_L(T/T_c) = B_{c2}(T/T_c)\left[1 - \frac{g}{A}\frac{T}{T_c}\left(1 - \frac{T}{T_c}\right)^{-1/2}\right], \qquad (1)$$

where $g=0.09-0.12$, A is a number of order unity, and B_{c2} is the upper critical field. The $B_L(T/T_c)$ curve is also shown as a solid line in Fig. 4, where $\xi_0=1.6$ nm, $\xi=0.74\xi_0(1\text{-}T/T_c)^{-1/2}$, and $g/A=0.14$ are used. The T_g/T_c-B curves of the present study also agree well with the $B_L(T/T_c)$ curve in Fig. 4. This shows that the sufficiently elongated c-axis correlated pinning centers achieve the upper limit of T_g/T_c, which is determined by the loss of line tension of vortices. This suggests that c-axis correlated pinning centers sufficiently optimize both the vortex configuration (straight one) and the pinning strength for each vortex if they are elongated through a thickness of a film. This is plausible from the viewpoint of the geometry of pinning centers.

For optimum doped YBCO ($T_c=92$ K), a B_L value at 77 K is 27 T. However, such a high T_g value has not been reported yet. In order to achieve it, T_c and B_Φ values should be improved in the YBCO containing the sufficiently elongated c-axis correlated pinning centers. It is well known that T_g/T_c starts to decrease rapidly at a B_Φ when a magnetic field increases.[17] Figure 4 shows that the T_g of the YBCO containing the sufficiently elongated c-axis correlated pinning centers corresponds to its upper limit in the low magnetic fields. These indicate that the crossover from the upper-limit T_g to non-upper-limit T_g occurs at a B_Φ. This is confirmed by an inset of Fig. 4, which shows that the T_g/T_c-B curve of the YBCO+BSO(4) SL deviates from the $B_L(T/T_c)$ curve (the upper limit of T_g/T_c) in magnetic fields above 3 T ($\sim B_\Phi$). This should be observed regardless of B_Φ values.[17] Thus, a B_Φ value should be enhanced to maintain the upper limit of T_g/T_c even in high magnetic fields. In addition, T_c should be enhanced to obtain a high T_g value at a given magnetic field. The T_c values in the YBCO+BMO (4) SLs of the present study (<90 K) are too low to achieve $B_L=27$ T in 77 K. By controlling the elongation of c-axis correlated pinning centers, T_c and a B_Φ, a T_g value of 77 K can be obtained in YBCO in a magnetic field as high as 27 T.

In conclusion, the control of T_g was discussed in YBCO films. The vortex configuration (entangled or straight) and the pinning strength for each vortex are crucial to the T_g/T_c behaviors. The sufficiently elongated c-axis correlated pinning centers can optimize these factors. Thus, the vortex pinning due to c-axis correlated pinning centers is effective enough to achieve the upper limit of T_g/T_c, which is given by the loss of line tension of vortices, if they are elongated through a thickness of a sample and an applied magnetic field is lower than a matching field. By optimizing the elongation of c-axis correlated pinning centers, T_c and a B_Φ, a T_g value of 77 K can be obtained in YBCO in a magnetic field as high as 27 T.

This work was supported by the CREST project of Japan Science and Technology Agency.

*matsu@post.matsc.kyutech.ac.jp

[1] G. Blatter, M. V. Feigel'man, V. B. Geshkenbein, A. I. Larkin, and V. M. Vinokur, Rev. Mod. Phys. **66**, 1125 (1994).
[2] D. R. Nelson and V. M. Vinokur, Phys. Rev. B **48**, 13060 (1993).
[3] S. A. Grigera, E. Morre, E. Osquiguil, C. Balseiro, G. Nieva, and F. de la Cruz, Phys. Rev. Lett. **81**, 2348 (1998).
[4] R. J. Olsson, W. K. Kwok, L. M. Paulius, A. M. Petrean, D. J. Hofman, and G. W. Crabtree, Phys. Rev. B **65**, 104520 (2002).
[5] D. S. Fisher, M. P. A. Fisher, and D. A. Huse, Phys. Rev. B **43**, 130 (1991).
[6] A. M. Petrean, L. M. Paulius, W. K. Kwok, J. A. Fendrich, and G. W. Crabtree, Phys. Rev. Lett. **84**, 5852 (2000).
[7] J. Figueras, T. Puig, X. Obradors, W. K. Kwok, L. Paulius, G. W. Crabtree, and G. Deutscher, Nat. Phys. **2**, 402 (2006).
[8] J. L. MacManus-Driscoll, S. R. Foltyn, Q. X. Jia, H. Wang, A. Serquis, L. Civale, B. Maiorov, M. E. Hawley, M. P. Maley, and D. E. Peterson, Nature Mater. **3**, 439 (2004).
[9] S. Kang, A. Goyal, J. Li, A. A. Gapud, P. M. Martin, L. Heatherly, J. R. Thompson, D. K. Christen, F. A. List, M. Paranthaman, and D. F. Lee, Science **311**, 1911 (2006).
[10] J. Gutierrez, A. Llordes, J. Gazquez, M. Gibert, N. Roma, S. Ricart, A. Pomar, F. Sandiumenge, N. Mestres, T. Puig, and X. Obradors, Nature Mater. **6**, 367 (2007).
[11] T. Horide, K. Matsumoto, P. Mele, A. Ichinose, R. Kita, M. Mukaida, Y. Yoshida, and S. Horii, Appl. Phys. Lett. **92**, 182511 (2008).
[12] T. Horide, K. Matsumoto, A. Ichinose, M. Mukaida, Y. Yoshida, and S. Horii, Supercond. Sci. Technol. **20**, 303 (2007).
[13] P. J. M. Woltgens, C. Dekker, J. Swuste, and H. W. de Wijn, Phys. Rev. B **48**, 16826 (1993).
[14] A. V. Samoilov, M. V. Feigel'man, M. Konczykowski, and F. Holtzberg, Phys. Rev. Lett. **76**, 2798 (1996).
[15] A. Mazilu, H. Safar, M. P. Maley, J. Y. Coulter, L. N. Bulaevskii, and S. Foltyn, Phys. Rev. B **58**, R8909 (1998).
[16] T. Nojima, M. Katakura, S. Okayasu, and N. Kobayashi, Physica C **378-381**, 593 (2002).
[17] L. Radzihovsky, Phys. Rev. Lett. **74**, 4923 (1995).